Scientific Research Publishing

Pharmacology & Pharmacy, 2024, 15, 347-363
https://www.scirp.org/journal/pp
ISSN Online: 2157-9431
ISSN Print: 2157-9423

Virtual Screening and Mechanism Analysis of Effective Components from Several Chinese Herbs to Inhibit dPLA2 of *Deinagkistrodon acutus* Venom

Hongbin Zhang, Xingyang Xiao, Mengyi Lai, Yi Gong, Jianzhong Huang*

Key Laboratory of Chronic Diseases, Fuzhou Medical University, Fuzhou, China
Email: *huangjz@whu.edu.cn

How to cite this paper: Zhang, H.B., Xiao, X.Y., Lai, M.Y., Gong, Y. and Huang, J.Z. (2024) Virtual Screening and Mechanism Analysis of Effective Components from Several Chinese Herbs to Inhibit dPLA2 of *Deinagkistrodon acutus* Venom. *Pharmacology & Pharmacy*, **15**, 347-363.
https://doi.org/10.4236/pp.2024.1511021

Received: October 11, 2024
Accepted: November 10, 2024
Published: November 13, 2024

Abstract

Objective: In folk and TCM clinical medicine, Chinese herbal medicine is used to treat snakebite and has good curative effect, but its active ingredients and mechanism are still unclear. In this study, virtual screening and mechanism analysis of effective components from 6 Chinese herbs to inhibit phospholipase A2 of *Deinagkistrodon acutus* (dPLA2) venom were conducted. **Methods:** With advanced computing software AutoDock, Pymol and GROMACS, the molecules selected from the Chinese herbal Medicine Chemical Composition databas6e (TCMSP) were docked with the dPLA2 from the protein database (PDB). Further molecular dynamics simulation was used to evaluate the molecular binding stability. **Results:** Four potential dPLA2-inhibiting molecules were screened: *lobelanidine*, *lobeline*, *norlobelanine* and *pratensein*, by analyzing the spatial structure, binding energy and binding interaction of small molecular-dPLA2 complexes, as well as the RMSD and RMSF of molecular dynamics simulation. **Conclusion:** To our knowledge, this is the first report of *lobeline* has an inhibitory effect on dPLA2, and *lobelanidine*, as a precursor of *lobeline*, has a stronger inhibitory effect. According to the docking results, it is speculated that the mechanism of action of the four molecules is to form stable interactions with calcium ions and amino acid residues on the calcium ion binding ring in dPLA2. Moreover, these small molecules compete with phosphatidylcholine (the natural substrate of dPLA2) to bind dPLA2 and have a higher affinity than phosphatidylcholine, resulting in inhibition of dPLA2 activity.

Keywords

Chinese Herbal Medicine, *Deinagkistrodon acutus* Phospholipase A2

*Corresponding author.

Inhibitor, Molecular Docking, Molecular Dynamics Simulation, Molecular Mechanism

1. Introduction

Deinagkistrodon acutus, also known as five-paced viper [1], is one of the most venomous snakes that have been seriously endangering the human health for a long time. The venom of the *D. acutus* primarily leads to coagulopathy and promotes tissue damage, necrosis, edema, hemorrhage, hemostatic imbalance, and acute renal failure [2], then causing massive death and permanent disability worldwide [3].

Snake venom is mainly composed of bioactive proteins and polypeptides (about 90% - 95%) [4]. Phospholipase A2 (PLA2), an important toxin in *D. acutus* venom, is a proteolytic enzyme that hydrolyzes phospholipids on the cell membrane, releases lysophospholipids, changes the permeability of the cell membrane [5], and leads to various pathological processes such as muscular toxicity, cardiotoxicity, neurotoxicity, hemolysis, edema and proinflammatory effects [6]. A large number of studies have confirmed that most antivenomous Chinese herbs achieve therapeutic purposes by inhibiting the action of PLA2.

Traditional Chinese medicine has a history of more than 2000 years in the treatment of snake wounds, and has accumulated rich experience. *Hedyotis diffusa* Willd [7], *Lobelia chinensis* Lour [8] [9], *Andrographis paniculata* Nees [10] [11], etc, are commonly used in the treatment of snake wounds in traditional Chinese medicine. Chinese herbal medicine plays an irreplaceable role in local treatment, reducing inflammation, inhibition activity on edema, hemorrhage, and lethality, and improving cure rate [12]-[15]. In order to make up for the shortcomings of common western medicines such as antivenoms, which are prone to side effects, difficult to obtain and preserve, lack of broad-spectrum effectiveness and inability to remove non-free snake venom, clinicians often use antivenoms combined with traditional Chinese medicine to treat snakebites, so as to achieve the purpose of complementary and synergistic [16]. It can be seen that the snake wound preparation of Chinese medicine, which is convenient to use and easy to store, has a wide application prospect.

In recent years, domestic and foreign scholars have found that a large number of plant extracts or their components can inhibit the activity of snake venom. For example, Luciana C. Diogo *et al*. found that the genetically modified component of *Eclipta prostata* can inhibit the myotoxic activity induced by basic PLA2 isolated from the venom of *Bothrops jararacussu* [17]. Junbo Chen *et al*. found that the aboveground extract of *Houttuynia cordata* Thunb had a significant inhibitory effect on dPLA2 activity [18]. Ren Yongshen *et al*. confirmed that the fresh juice concentrate of *Sedum sarmentosum* Bunge has a more significant antivenom effect than the dry water extract or alcohol extract [19].

With the gradual standardization of snakebite treatment, further research on the pharmacological mechanism of Chinese herbal medicine treatment of snakebite has become an inevitable trend. According to the current research results, the composition and mechanism of the direct inactivation effect of Chinese herbal medicine on snake venom are not clear [15]. Based on this, this study took dPLA2 as the research object, and used molecular docking and molecular dynamics simulation techniques to screen six active components of Chinese herbal medicine, analyze the interaction mechanism between small molecules and dPLA2, and provide a basis for the treatment of venomous snakebite and the development of snake venom inhibitors.

2. Materials and Methods

2.1. Materials

The molecular docking software is Autodock vina (https://autodock.scripps.edu); The visual processing software uses the open-source version of Pymol2.1 (Archived: Python Extension Packages for Windows-Christoph Gohlke (uci.edu)); GROMACS (https://www.gromacs.org/) is used for molecular dynamics simulation. TCMSP-Traditional Chinese Medicine Systems Pharmacology Database and Analysis Platform (tcmsp-e.com); Protein Database (RCSB PDB: Homepage) and Discovery studio visualizer (Free Download: BIOVIA Discovery Studio Visualizer-Dassault Systemes (3ds.com)).

2.2. Preparation dPLA2 and Small Molecules for Docking

dPLA2 protein crystal structure (PDB ID: 1ijl) was retrieved from the PDB database and downloaded as a receptor; The six Chinese herbs selected for study are *Hedyotis diffusa* Willd, *Lobelia chinensis* Lour, *Andrographis paniculata* Nees, *Houttuynia cordata* Thunb, *Sedum sarmentosum* Bunge, *Eclipta prostata*. All the molecular components of these herbs were obtained from the TCMSP database, and screened according to bioavailability OB ≥ 30% and drug properties DL ≥ 0.18. The 3D structure of the selected small molecules was downloaded as ligands for docking with the PLA2 of *Deinagkistrodon acutus*.

2.3. Visual Processing the Results of Molecular Docking

The small molecule and dPLA2 protein were dehydrated and hydrogenated, respectively, and the small molecule twisting bond was detected before molecular docking; The processed small molecules and proteins were imported into Autodock software [20]. The docking site refers to the smallest spatial extent that encompasses the active center of the receptor. This encompasses the area defined by the docking box during the operation. Consequently, the size and the center coordinates of the box serve as a representation of this range throughout the procedure. The active site of dPLA2 comprises the region delineated by residues Y27, G29, G31, H47, D48, and D89. Consequently, we established the docking site with central coordinates at X = 8.391401, Y = 11.560492, Z = 47.501534, and size of 15 ×

15 × 15. Then initiating molecular docking; The docking result files are saved in pdbqt and pdb formats; The former was imported into PYMOL [21] for visualized, the latter imported the Discovery studio visualizer to analyze the receptor-ligand interaction and derive the 2D diagram of the interaction [22]; After docking, the results obtained were compared with the selected reference (phosphatidylcholine and gallic acid) in terms of binding site, binding energy, hydrogen bonding, etc.

2.4. Molecular Dynamics Simulation

GROMACS software was used for molecular dynamics simulation [23]. First, the ligand and receptor were separated from the docking result file, and the charge information was added separately to form two independent files. Secondly, topological files of ligand and receptor are generated, respectively. Then the atom information of the ligand topological file is integrated with the information of the receptor topological file to form the complex topological file, and the solvent is added to the complex topological file to generate the constraint box. After that, charge detection, balance charge, energy minimization, nvt balance and npt balance were carried out. Finally, dynamic simulation was carried out, and the simulation time was set to 100 ns. The changes of RMSD and RMSF values and the number of hydrogen bonds of complex and receptor were analyzed respectively.

3. Results

3.1. Screening of Potential Active Ingredients of 6 Antivenom Chinese Herbal Medicines

Oral bioavailability (OB) and drug-like properties (DL) are two important basic parameters for virtual screening of small molecules with potential pharmacological effects. Using OB ≥ 30% and DL ≥ 0.18 as criteria, 287 molecules of 6 Chinese herbs were screened, and a total of 60 components were obtained. The results were shown in **Table 1**. Molecular docking of these 60 compounds was performed. As shown in **Table 1**, it is known that the lower the binding energy, the more stable the ligand-receptor binding is. The binding energy of all 60 compounds is less than 0, indicating that they can all bind to dPLA2. Among them, the binding energy of 53 small molecules was lower than that of *gallic acid* (−6.3 kJ/mol), and 59 small molecules was lower than phosphatidylcholine. Among the 10 small molecules with the lowest binding energy, 5 were from *Lobelia chinensis*, 2 were from *Hedyotis diffusa*, and there was 1 species of *Houttuynia cordata*, *Sedum sarmentosum*, *Eclipta prostata* respectively.

3.2. Molecular Docking of the Screened Potential Active Ingredients with dPLA2

3.2.1. Binding Energy Analysis of Molecular Docking

Since the lower the binding energy, the more stable the binding is, the 10 small molecules with the lowest binding energy among the 60 small molecules were

Table 1. Results of screening and molecular docking.

MOLID	Name	Herb	Affinity
MOL008290	1,2-diacyl-sn-glycero-3-phosphocholine	substrate	−5.7
MOL000513	Gallic acid	positive control	−6.3
MOL012207	lobelanidine	Lobeliae Chinensis Herba	−9.3
MOL004355	Spinasterol	Houttuyniae Herba	−9.2
MOL012209	Lobeline	Lobeliae Chinensis Herba	−9.1
MOL012216	norlobelanine	Lobeliae Chinensis Herba	−9.0
MOL000449	Stigmasterol	Hedyotis Diffusae Herba	−8.9
MOL001659	Poriferasterol	Hedyotis Diffusae Herba	−8.8
MOL001792	DFV	Sedi Herba	−8.8
MOL003398	Pratensein	Ecliptae Herba	−8.8
MOL009653	Cycloeucalenol	Lobeliae Chinensis Herba	−8.8
MOL012208	Lobelanine	Lobeliae Chinensis Herba	−8.7
MOL001670	2-methoxy-3-methyl-9,10-anthraquinone	Hedyotis Diffusae Herba	−8.6
MOL003389	3'-O-Methylorobol	Ecliptae Herba	−8.6
MOL002975	butin	Ecliptae Herba	−8.6
MOL001689	acacetin	Lobeliae Chinensis Herba, Ecliptae Herba	−8.5
MOL002341	Hesperetin	Lobeliae Chinensis Herba	−8.5
MOL000422	kaempferol	Lobeliae Chinensis Herba, Houttuyniae Herba	−8.3
MOL002881	Diosmetin	Lobeliae Chinensis Herba	−8.3
MOL002928	oroxylin a	Andrographis Herba	−8.3
MOL003044	Chryseriol	Lobeliae Chinensis Herba	−8.3
MOL011678	(3S,8S,9S,10R,13R,14S,17R)-17-[(1S,4R)-4-ethyl-1,5-dimethylhexyl]-10,13-dimethyl-2,3,4,7,8,9,11,12,14,15,16,17-dodecahydro-1H-cyclopenta[a]phenanthren-3-ol	Lobeliae Chinensis Herba	−8.3
MOL000006	luteolin	Lobeliae Chinensis Herba, Ecliptae Herba, Sedi Herba	−8.2
MOL000358	beta-sitosterol	Lobeliae Chinensis Herba, Hedyotis Diffusae Herba	−8.2
MOL004350	Ruvoside_qt	Houttuyniae Herba	−8.2
MOL000098	quercetin	Lobeliae Chinensis Herba, Ecliptae Herba, Hedyotis Diffusae Herba, Sedi Herba	−8.1
MOL008209	Deoxycamptothecine	Andrographis Herba	−8.1
MOL003851	Isoramanone	Houttuyniae Herba	−8.0
MOL008217	Paniculogenin	Andrographis Herba	−8.0
MOL008239	Quercetin tetramethyl (3',4',5,7) ether	Andrographis Herba	−8.0
MOL000354	isorhamnetin	Sedi Herba	−7.9
MOL003402	demethylwedelolactone	Ecliptae Herba	−7.8

Continued

MOL005530	Hydroxygenkwanin	Lobeliae Chinensis Herba	−7.8
MOL008219	3-[2-[(1R,4aS,5R,8aS)-5,8a-dimethyl-2-methylene-5-methylol-decalin-1-yl]ethyl]-5H-furan-2-one	Andrographis Herba	−7.8
MOL003378	1,3,8,9-tetrahydroxybenzofurano[3,2-c]chromen-6-one	Ecliptae Herba	−7.7
MOL008215	Paniculide B	Andrographis Herba	−7.7
MOL008232	(3Z,4S)-3-[2-[(1R,4aS,5R,6R,8aS)-6-hydroxy-5,8a-dimethyl-2-methylene-5-methylol-decalin-1-yl]ethylidene]-4-hydroxy-tetrahydrofuran-2-one	Andrographis Herba	−7.6
MOL008238	3-[2-[(1S,4aR,5S,8aR)-5,8a-dimethyl-2-methylene-5-methylol-decalin-1-yl]ethyl]-5H-furan-2-one	Andrographis Herba	−7.6
MOL000173	wogonin	Andrographis Herba	−7.5
MOL001790	Linarin	Lobeliae Chinensis Herba, Ecliptae Herba	−7.5
MOL002932	Panicolin	Andrographis Herba	−7.4
MOL008222	andrographidine B_qt	Andrographis Herba	−7.4
MOL008216	Paniculide C	Andrographis Herba	−7.4
MOL008226	14-deoxyandrographolide	Andrographis Herba	−7.4
MOL003404	wedelolactone	Ecliptae Herba	−7.3
MOL009009	(+)-medioresinol	Lobeliae Chinensis Herba	−7.2
MOL008206	Moslosooflavone	Andrographis Herba	−7.1
MOL012225	3-[(2S,3R)-2-(4-hydroxy-3-methoxy-phenyl)-3-(hydroxymethyl)-7-methoxy-2,3-dihydrobenzofuran-5-yl] propyl acetate	Lobeliae Chinensis Herba	−7.1
MOL008228	Andrographin	Andrographis Herba	−6.6
MOL008234	andrographolide-19-β-D-glucoside_qt	Andrographis Herba	−6.6
MOL001646	2,3-dimethoxy-6-methyanthraquinone	Hedyotis Diffusae Herba	−6.5
MOL008218	1-Monoolein	Andrographis Herba	−6.5
MOL008223	andrographidine C	Andrographis Herba	−6.5
MOL008204	Mono-O-methylwightin	Andrographis Herba	−6.4
MOL008213	14-deoxy-12-methoxyandrographolide	Andrographis Herba	−6.4
MOL008203	14-deoxy-11-oxo-andrographolide	Andrographis Herba	−6.2
MOL001663	(4aS,6aR,6aS,6bR,8aR,10R,12aR,14bS)-10-hydroxy-2,2,6a,6b,9,9,12a-heptamethyl-1,3,4,5,6,6a,7,8,8a,10,11,12,13,14b-tetradecahydropicene-4a-carboxylic acid	Hedyotis Diffusae Herba	−6.1
MOL008230	andrographidine F_qt	Andrographis Herba	−6.0
MOL004351	C09747	Houttuyniae Herba	−5.9
MOL008210	Deoxyelephantopin	Andrographis Herba	−5.9
MOL004345	1-methyl-2-nonacosyl-4-quinolone	Houttuyniae Herba	−5.8
MOL008229	Andrographin F	Andrographis Herba	−5.6

mainly selected for interaction analysis. The 10 small molecules were *lobelanidine* (−9.3 kJ/mol), *Spinasterol* (−9.2 kJ/mol), *Lobeline* (−9.1 kJ/mol), *norlobelanine* (−9.0 kJ/mol), *Stigmasterol* (−8.9 kJ/mol), *Poriferasterol* (−8.8 kJ/mol) and DFV (−8.8 kJ/mol), *Pratensein* (−8.8 kJ/mol), *Cycloeucalenol* (−8.8 kJ/mol), *Lobelanine* (−8.7 kJ/mol), and the docking interactions were shown in Table 2. The binding energy of 10 small molecules was lower than that of *gallic acid* (−6.3 kJ/mol). *Lobelanidine* was the lowest and *Lobelanine* was the highest, and there was no significant difference between them.

Table 2. Interaction results of the top 10 small molecules with dPLA2.

MOLID	hydrogen bond	hydrophobic	Charge	The interaction with the Ca	Other interactions
MOL008290	TRP30GLY31 HIS47 LYS60	CYS44 HIS47 PRO120	TRP30 LYS60	/	C-H:GLY32
MOL000513	TYR21 GLY29 ASP48	PHE5 HIS47	/	Metal-Acceptor	/
MOL012207	GLY27 GLY29 ASP48	LEU2 TRP30	ASP48	Unfavorable Metal-Donor	/
MOL004355	ASP48	LEU2, PHE5, ILE9, TRP20, TRP30, CYS44, HIS47, TYR51, LYS60, PHE96	/	/	/
MOL012209	GLY29 GLY31	LEU2, PHE5, TRP30, CYS44, HIS47	ASP48	Metal-Acceptor	
MOL012216	GLY29 GLY31 ASP48	LEU2, PHE5, TRP30	ASP48	Metal-Acceptor	C-H:CYS28
MOL000449	TYR21	LEU2, PHE5, TRP20, TRP30, HIS47, PRO59, TYR51, LYS60	/	/	/
MOL001659	TYR21	LEU2, PHE5, TRP20, TRP30, HIS47, PRO59, TYR51, LYS60	/	/	/
MOL001792	TYR21	LEU2, PHE5, TRP20, TRP30, HIS47, PRO59, TYR51, LYS60	/	/	/
MOL003398	CYS44 GLY31 LYS60	PHE5, CYS44, HIS47	Ca	Metal-Acceptor	C-H:CYS28
MOL009653	ASP48	LEU2, PHE5, ILE9, TRP20, TRP30, CYS44, HIS47, TYR51, PHE96	/	/	/
MOL012208	GLY31	LEU2, PHE5, TRP30, HIS47	ASP48	/	C-H:CYS28

3.2.2. Comparison of Spatial Structure and Bonding of Molecular Docking

The number of hydrogen bonds is an important factor in determining the stability of ligand binding. As shown in Table 2, *lobelanidine*, *norlobelanine* and *Pratensein* form hydrogen bonds with three amino acid residues of dPLA2 respectively, *lobeline* forms hydrogen bonds with two amino acid residues of dPLA2, and the other molecules have only one hydrogen bond. Therefore, four small molecules were selected according to the number of hydrogen bonds, which were *lobelanidine*, *norlobelanine*, *Pratensein and lobeline*.

The docking results of four small molecules were visualized, as shown in Figure 1. From the comparison of the overall spatial structure of the four small molecules and dPLA2 complex, it can be seen that They are all bound in the same surface pocket of dPLA2, which is formed by the calcium ion binding ring (TYR27, GLY29, GLY31, ASP48), calcium ion and its surrounding amino acids, and the surface pocket is the same as the *gallic acid* and phosphatidylcholine binding active pocket, with similar binding orientation of the four molecules, as shown in Figure 2.

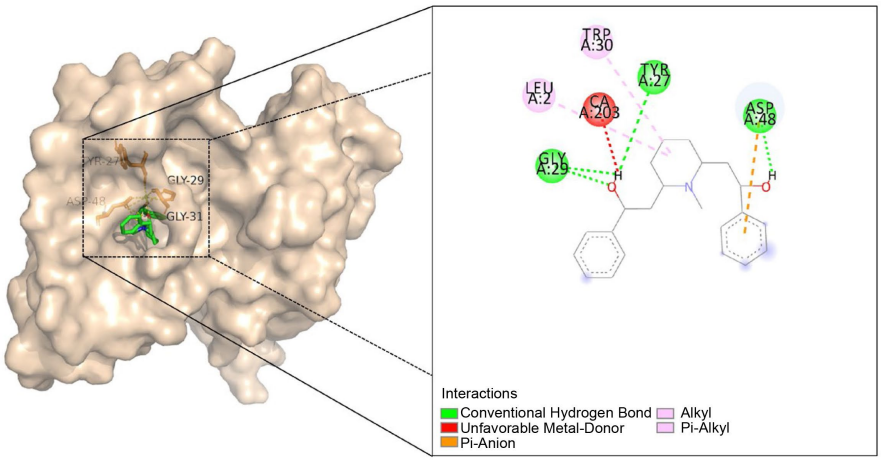

(a)

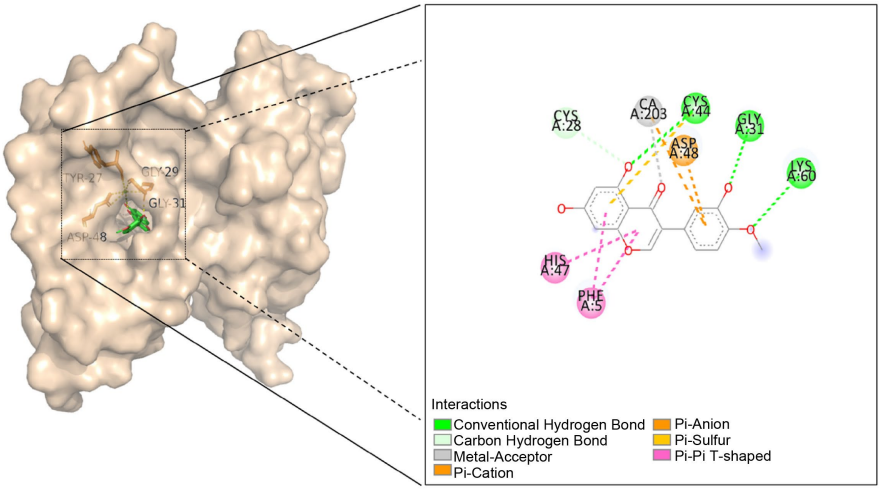

(b)

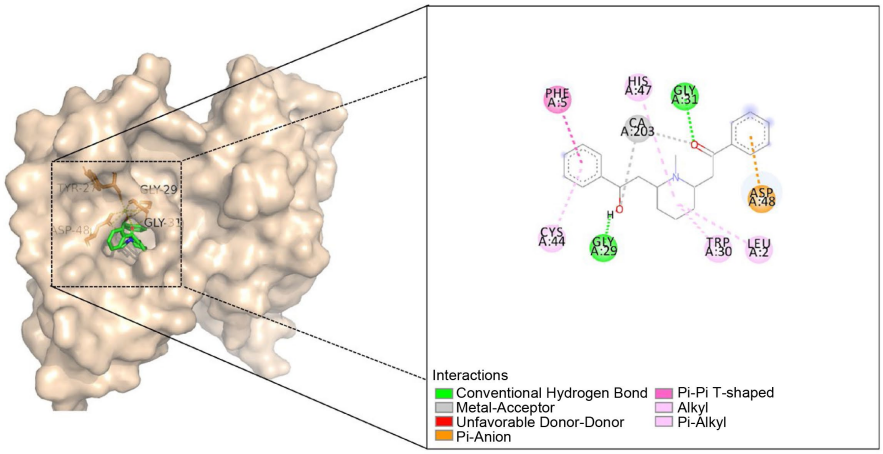

(c)

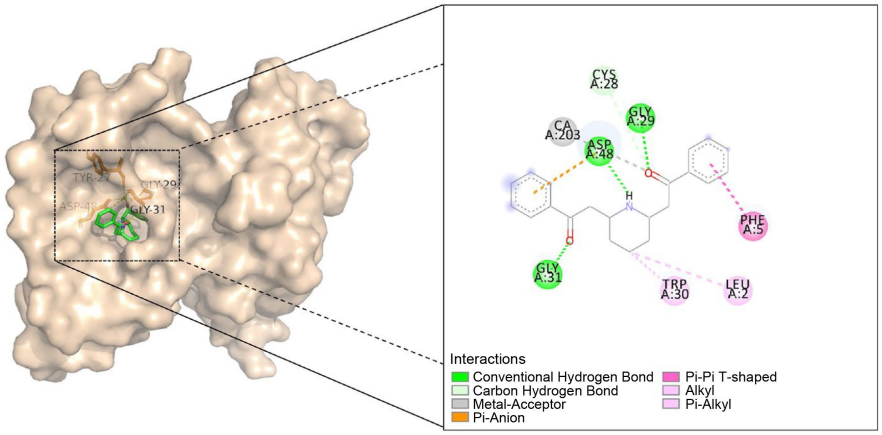

(d)

Figure 1. Depicts the docking outcomes of four pivotal active constituents with dPLA2. Specifically, 1a exemplifies the interplay between *Pratensein* and dLPA2, 1b showcases the interaction between *lobelanidine* and dLPA2, 1c portrays the engagement between *Lobeline* and dLPA2, and 1d illustrates the association between *norlobelanine* and dLPA2.

From the comparison of interactions, it can be seen that, on the one hand, the docking interaction results of the four small molecules are similar to *gallic acid*: they all interact with calcium ions; *lobelanidine*, *norlobelanine* and *gallic acid* form hydrogen bonds with GLY29 and ASP48; *Lobeline* and *gallic acid* form hydrogen bonds with GLY31; *Lobelin*, *Pratensein* and *gallic acid* all have hydrophobic effects with PHE5 and HIS47. On the other hand, phosphatidylcholine is a natural substrate for dPLA2 and binds to the active center of dPLA2. By analyzing the hydrogen bond and hydrophobic action of phosphatidylcholine, *lobelanidine*, *norlobelanine*, *Pratensein and lobeline* binding with dPLA2, it was found that GLY31 and LYS60 of dPLA2 were involved in the binding with phosphatidylcholine. And there were hydrogen bonds between *Pratensein* and these two amino acids; *Norlobelanine and lobeline* form hydrogen bonds with GLY31; *Lobelanidine* does not interact with either of them; And *Lobeline*, *Pratensein* and phosphatidylcholine all form hydrophobic interactions with CYS44 and HIS47.

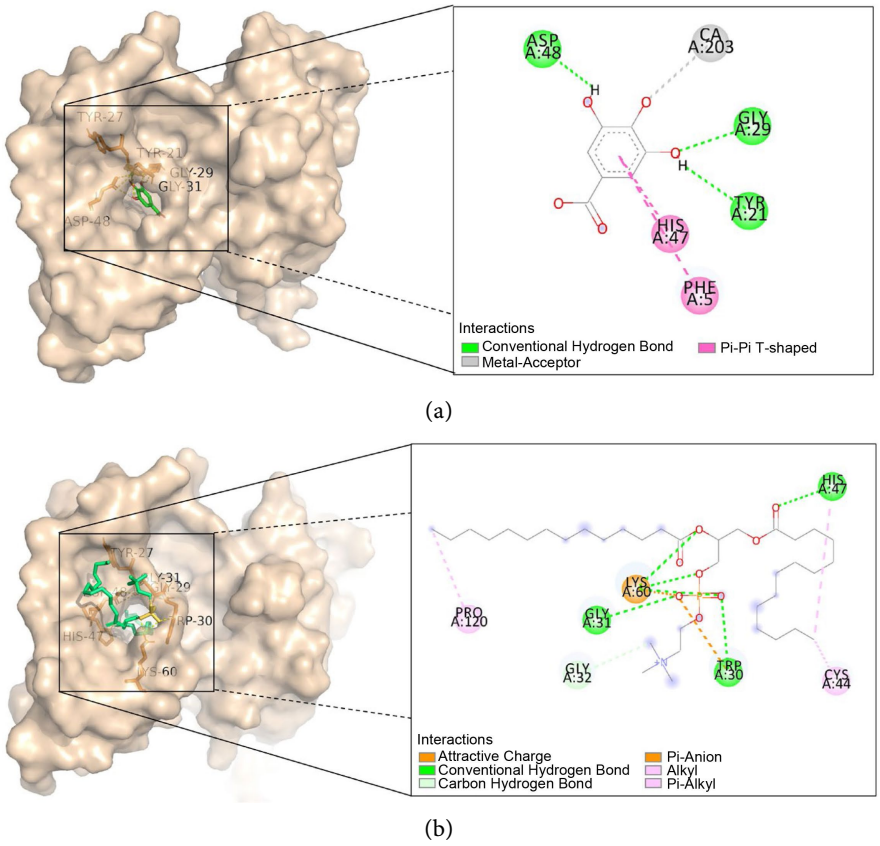

Figure 2. *Gallic acid* and phosphatidylcholine docking outcomes with dPLA2, respectively.

Through the interaction analysis, *Lobeline*, *norcloberanine*, *Pratensein and lobelanidine* all had the possibility of inhibiting dPLA2.

3.3. Molecular Dynamics Simulation

Molecular dynamics is a set of molecular simulation methods widely used in physics, chemistry, biology, materials, medicine and other fields. This method mainly relies on Newtonian mechanics to simulate the motion of the molecular system, and extracts samples from the system composed of different states of the molecular system, so as to calculate the configuration integral of the system, and further calculate the thermodynamic quantity and other macroscopic properties of the system based on the results of the configuration integral. The stability of ligand-binding receptors can be evaluated more directly through molecular dynamics simulation of protein-ligand complexes.

Root mean square deviation (RMSD) and root mean square fluctuation (RMSF) are two important parameters in molecular dynamics simulation. They represent the mean difference between the complex conformation during the simulation time and the initial complex conformation, and the mean deviation between the atomic position of the complex during the simulation time and its initial position. Respectively reflecting the stability of the overall conformation of the complex and the flexibility of the overall structure. Based on these two parameters, the stability

of dPLA2 binding to four small molecules was verified in this study.

3.3.1. RMSD Analysis

Figure 3(a) shows the curve comparison of RMSD values of the four complexes

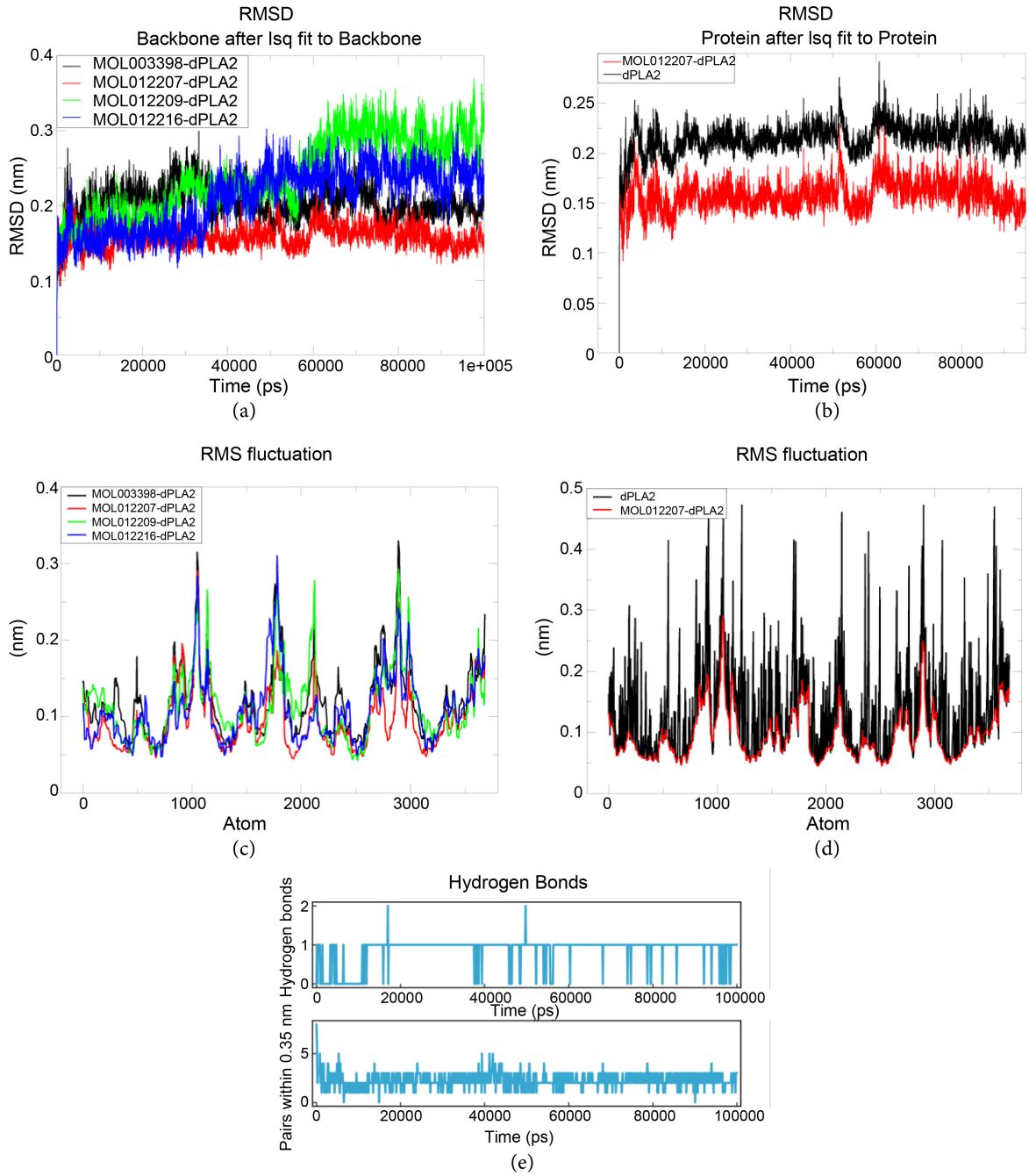

Figure 3. Results of molecular dynamics simulation. (a) presents a comparative graph illustrating the RMSD (Root Mean Square Deviation) values of four potential complexes across the simulation timeline. (b) displays a comparative chart depicting the RMSD values of the dPLA2 and MOL012207-dPLA2 complex over the course of the simulation. (c) showcases a comparative graph of the RMSF (Root Mean Square Fluctuation) values of the four candidate complexes throughout the simulation period. (d) features a comparative chart of the RMSF values of the dPLA2 and MOL012207-dPLA2 complex during the simulation. Lastly, (e) presents a chart outlining the number of hydrogen bonds present in the MOL012207-dPLA2 complex as the simulation progresses.

over the simulation time. It can be seen from the figure that the RMSD values of the four compounds tend to converge after 100 ns simulation, and their RMSD values are all lower than 4 ns. The *lobelanidine* curve is the most stable, and the RMSD value as a whole is lower than 0.2 ns, indicating that *lobelanidine* binding stability is the strongest. It was followed by *Pratensein Lobeline*, *norcloberanine*. Figure 3(b) shows the comparison of RMSD value of *lobelanidine*-dPLA2 complex and dPLA2. It can be seen from the figure that the RMSD value of *lobelanidine*-dPLA2 complex is lower than dPLA2 on the whole, indicating that the stability of dPLA2 combined with *lobelanidine* is enhanced.

3.3.2. RMSF Analysis

Figure 3(c) shows the comparison of the RMSF values of the four complexes with the number of atoms. It can be seen from the figure that the RMSF values of the atoms of the four complexes are all lower than 0.35 nm, among which *lobelanidine*-dPLA2 complex has the lowest RMSF value as a whole and is located below other curves, indicating that the complex has the lowest overall flexibility and the most stable structure. Figure 3(d) is a comparison of RMSF curves of *lobelanidine*-dPLA2 complex and dPLA2. It can be seen from the figure that the RMSF curve of *lobelanidine*-dPLA2 complex as a whole is below the RMSF curve of dPLA2, indicating that the flexibility of dPLA2 combined with *lobelanidine* is weakened and the structural stability of the complex is enhanced.

3.3.3. Hydrogen Bond Analysis

Lobelanidine showed the best stability in both RMSD and RMSF analysis, so the hydrogen bond analysis of *Lobelanidine* was mainly performed. Figure 3(e) shows the variation in the number of hydrogen bonds between *Lobelanidine* and dPLA2 over the simulation time. It can be seen from the figure that the number of hydrogen bonds remained at 1 overall during the simulation time. In addition, When the distance between ligand and receptor is less than 0.35 nm, 3 pairs of hydrogen bonds are maintained, which is consistent with the molecular docking results.

4. Discussion

4.1. Mechanism of Interaction between Small Molecules and dPLA2

dPLA2 is a calcium-dependent acid hydrolase, which mainly causes tissue hemolysis and edema [24]. The reason is that dPLA2 produces arachidonic acid by hydrolyzing phosphatidylcholine on red blood cell membranes, and the arachidonic acid is metabolized to produce inflammatory mediators such as prostaglandin, thrombin and leukotriene, which cause further hemolysis, vasodilation, increased vascular permeability, and finally tissue edema. On this basis, we identified molecules that potentially inhibit the hydrolysis of phosphatidylcholine by dPLA2 in order to block the hemolytic reaction and tissue edema.

The methods of inhibiting dPLA2 and small molecule binding sites are closely

related. Studies have shown that dPLA2 binding sites are TYR27, GLY29, GLY31 and ASP48, and active sites are HIS47 and ASP89 [24]. Accordingly, dPLA2 interacts with phosphatidylcholine and gallic acid, respectively; the docking results are shown in **Figure 1** and **Table 1**. The comparison of the docking results showed that the surface parts of *gallic acid* and phosphatidylcholine binding dPLA2 were the same as those in the spatial structure analysis. The binding energies of *gallic acid* and phosphatidylcholine were −6.3 kJ/mol and −5.7 kJ/mol, respectively, and the lower the binding energies were, the stronger the binding affinity was. Therefore, the binding affinity of *gallic acid* and dPLA2 was stronger than that of phosphatidylcholine. From the interaction analysis, both *gallic acid* and phosphatidylcholine were bound to dPLA2 binding sites, but the binding amino acids were different. *Gallic acid* was bound to GLY29 and ASP48, and phosphatidylcholine was bound to GLY31, and both of them formed hydrophobic interaction with HIS47. In addition, phosphatidylcholine binds to the active site HIS47, but *gallic acid* does not bind to the active site, and *gallic acid* forms metallic bonds with calcium ions, but phosphatidylcholine does not bind to calcium ions. Therefore, we speculated that binding to the binding site is the basis of the effect of small molecules on dPLA2 activity, and binding to calcium ions may inhibit dPLA2.

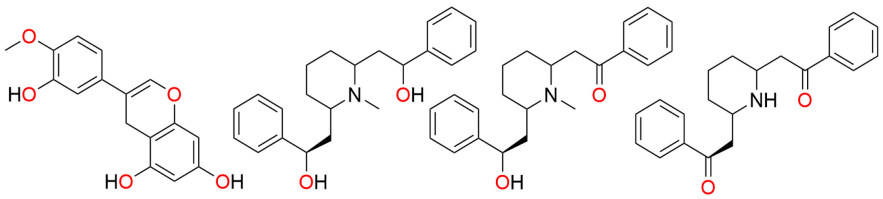

Figure 4. Structures of *pratensein*, *lobelanidine*, *lobeline* and *norlobelanine*.

4.2. Four Valuable Small Molecules of Chinese Herbs

Through molecular docking and molecular dynamics simulation, we obtained four potential dPLA2 inhibition molecules, *lobelanidine*, *lobeline*, *norlobelanine* and *pratensein*. The structural formulas of four small molecules are shown in **Figure 4**. *lobelanidine*, *lobeline*, *norlobelanine* were all derived from *Lobelia chinensis*, and their structures were highly similar. The binding energy of the four small molecules were higher than that of *gallic acid* and phosphatidylcholine, and all of them were bound to dPLA2 binding sites and calcium ions but were not bound to HIS47 and ASP89, and their interaction characteristics were consistent with those of *gallic acid*. It is speculated that the molecular mechanism of its action is small molecules competitively inhibits the binding of dPLA2 with phosphatidylcholine, and is at an advantage in the competition, resulting in the overall inhibitory effect of dPLA2. Moreover, through molecular dynamics simulation, we found that the overall spatial conformation of four small molecules and dPLA2 complexes changed little and the overall flexibility decreased before and after simulation, indicating that the combination of small molecules and dPLA2 was stable.

As a respiratory stimulant, *lobeline* is widely used in clinical practice for

neonatal asphyxia, asphyxia caused by carbon monoxide, intoxication of inhaled anesthetic and other central depressants (such as opioids and barbiturates), and respiratory failure caused by infectious diseases such as pneumonia and diphtheria, with mild side effects [25] [26]. In addition, studies have shown that *lobeline* can also affect learning and memory [27], reduce depression-like behavior induced by nicotine withdrawal [28] [29], reduce alcohol dependence [30] [31], and reduce the function and metabolism of dopamine in the midbrain induced by alcohol in mice [32] [33]. *Lobelanidine* and *norlobelanine* are highly similar in structure to *lobeline*. For *pratensein*, studies have shown that it can reduce Aβ-induced oxidative damage and restore synaptic function [34]-[37]. Although these molecules are widely used in the treatment of diseases, there are no reports that they have inhibitory effects on dPLA2. To our knowledge, this is the first report of *Lobelanidine*, *lobeline*, *norlobelanine* and *pratensein* have an inhibitory effect on dPLA2, among which *Lobelanidine* had the strongest inhibitory effect. However, the actual inhibitory effect of these molecules on dPLA2 needs to be confirmed by further experiments.

Funding

This study was funded by The Science and Technology Research Project of Jiangxi Provincial Department of Education (GJJ2203420).

Conflicts of Interest

The authors declare no conflicts of interest regarding the publication of this paper.

References

[1] Nie, X., He, Q., Zhou, B., Huang, D., Chen, J., Chen, Q., *et al.* (2021) Exploring the Five-Paced Viper (*Deinagkistrodon acutus*) Venom Proteome by Integrating a Combinatorial Peptide Ligand Library Approach with Shotgun LC-MS/MS. *Journal of Venomous Animals and Toxins including Tropical Diseases*, **27**, e20200196. https://doi.org/10.1590/1678-9199-jvatitd-2020-0196

[2] Huang, J., Zhao, M., Xue, C., Liang, J. and Huang, F. (2022) Analysis of the Composition of *Deinagkistrodon acutus* Snake Venom Based on Proteomics, and Its Antithrombotic Activity and Toxicity Studies. *Molecules*, **27**, Article 2229. https://doi.org/10.3390/molecules27072229

[3] Avella, I., Schulte, L., Hurka, S., Damm, M., Eichberg, J., Schiffmann, S., *et al.* (2024) Proteogenomics-Guided Functional Venomics Resolves the Toxin Arsenal and Activity of *Deinagkistrodon acutus* Venom. *International Journal of Biological Macromolecules*, **278**, Article 135041. https://doi.org/10.1016/j.ijbiomac.2024.135041

[4] Costa, T.R., Francisco, A.F., Cardoso, F.F., Moreira-Dill, L.S., Fernandes, C.A.H., Gomes, A.A.S., *et al.* (2021) Gallic Acid Anti-Myotoxic Activity and Mechanism of Action, a Snake Venom Phospholipase A2 Toxin Inhibitor, Isolated from the Medicinal Plant Anacardium Humile. *International Journal of Biological Macromolecules*, **185**, 494-512. https://doi.org/10.1016/j.ijbiomac.2021.06.163

[5] Terra, A.L.C., Moreira-Dill, L.S., Simões-Silva, R., Monteiro, J.R.N., Cavalcante, W.L.G., Gallacci, M., *et al.* (2015) Biological Characterization of the Amazon Coral

Micrurus Spixii Snake Venom: Isolation of a New Neurotoxic Phospholipase A2. *Toxicon*, **103**, 1-11. https://doi.org/10.1016/j.toxicon.2015.06.011

[6] Cedro, R.C.A., Menaldo, D.L., Costa, T.R., Zoccal, K.F., Sartim, M.A., Santos-Filho, N.A., *et al*. (2018) Cytotoxic and Inflammatory Potential of a Phospholipase A2 from *Bothrops jararaca* Snake Venom. *Journal of Venomous Animals and Toxins including Tropical Diseases*, **24**, Article No. 33. https://doi.org/10.1186/s40409-018-0170-y

[7] Huang, L., Chen, B.L., Luo, L., *et al*. (2023) Research Advances in Chemical Components Pharmacological Activities and Clinical Application of Hedyotis Diff Usa. *China Pharmaceutical*, **37**, 1451-1460.

[8] Luo, J., Chen, Q., Li, P., Yu, H., Yu, L., Lu, J., *et al*. (2024) Lobelia Chinensis Lour Inhibits the Progression of Hepatocellular Carcinoma via the Regulation of the PTEN/AKT Signaling Pathway in Vivo and *in Vitr*o. *Journal of Ethnopharmacology*, **318**, Article 116886. https://doi.org/10.1016/j.jep.2023.116886

[9] Qiu, J., Chen, J., Wei, Y., Li, Y., Li, H., Wang, Z., *et al*. (2023) Chemical Constituents from *Lobelia davidii* Franch. and Their Chemotaxonomic Significance. *Biochemical Systematics and Ecology*, **108**, Article 104650. https://doi.org/10.1016/j.bse.2023.104650

[10] Lekshmi, P. and Unnikrishna, P.P. (2023) *In Vitro* Effect of Colchiploidy on Andrographolide Enhancement in *Andrographis paniculata* (Burm.f.) Wall. ex. Nees. *South African Journal of Botany*, **163**, 786-793.

[11] Zeng, B., Wei, A., Zhou, Q., Yuan, M., Lei, K., Liu, Y., *et al*. (2021) Andrographolide: A Review of Its Pharmacology, Pharmacokinetics, Toxicity and Clinical Trials and Pharmaceutical Researches. *Phytotherapy Research*, **36**, 336-364. https://doi.org/10.1002/ptr.7324

[12] Toyama, D.d.O., Gaeta, H.H., Pinho, M.V.T.d., Ferreira, M.J.P., Romoff, P., Matioli, F.F., *et al*. (2014) An Evaluation of 3-Rhamnosylquercetin, a Glycosylated Form of Quercetin, against the Myotoxic and Edematogenic Effects of Spla2fromcrotalus *Durissus terrificus*. *BioMed Research International*, **2014**, 1-11. https://doi.org/10.1155/2014/341270

[13] Gopi, K., Anbarasu, K., Renu, K., Jayanthi, S., Vishwanath, B.S. and Jayaraman, G. (2016) Quercetin-3-O-Rhamnoside from Euphorbia Hirta Protects against Snake Venom Induced Toxicity. *Biochimica et Biophysica Acta* (*BBA*)—*General Subjects*, **1860**, 1528-1540. https://doi.org/10.1016/j.bbagen.2016.03.031

[14] Sachetto, A.T.A., Rosa, J.G. and Santoro, M.L. (2018) Rutin (Quercetin-3-Rutinoside) Modulates the Hemostatic Disturbances and Redox Imbalance Induced by Bothrops Jararaca Snake Venom in Mice. *PLOS Neglected Tropical Diseases*, **12**, e0006774. https://doi.org/10.1371/journal.pntd.0006774

[15] Dong, D.G., Song, M., Deng, Z.P., *et al*. (2020) Research Progress on Local Tissue Damage of Snake Venom and Intervention of Plant Medicine. *Chinese Pharmacological Bulletin*, **36**, 907-911.

[16] Gutiérrez, J.M., León, G. and Burnouf, T. (2011) Antivenoms for the Treatment of Snakebite Envenomings: The Road Ahead. *Biologicals*, **39**, 129-142. https://doi.org/10.1016/j.biologicals.2011.02.005

[17] Diogo, L.C., Fernandes, R.S., Marcussi, S., Menaldo, D.L., Roberto, P.G., Matrangulo, P.V.F., *et al*. (2009) Inhibition of Snake Venoms and Phospholipases A2 by Extracts from Native and Genetically Modified Eclipta Alba: Isolation of Active Coumestans. *Basic & Clinical Pharmacology & Toxicology*, **104**, 293-299. https://doi.org/10.1111/j.1742-7843.2008.00350.x

[18] Chen, J.B., Yu, X.D., Xiong, Y., *et al*. (2022) Comparation of the Inhibitory Effects of

Extracts from Aerial Part and Root of Houttuynia Cordata Thunb on Deinagkistrodon Acutus Venom. *Acta scientiarum naturalium universtatis sunyatseni*, **61**, 35-44.

[19] Ren, Y.S., Zhang, T.P., Liang, S., *et al*. (2020) The Efficacy Superiority of Fresh Sedum Sarmentosum on Snakebite Treatment. *Journal of South-Central University for Nationalities* (*Natural Science Edition*), **39**, 151-156.

[20] Trott, O. and Olson, A.J. (2009) Autodock Vina: Improving the Speed and Accuracy of Docking with a New Scoring Function, Efficient Optimization, and Multithreading. *Journal of Computational Chemistry*, **31**, 455-461. https://doi.org/10.1002/jcc.21334

[21] Schrödinger, L. and DeLano, W. (2020) PyMOL. http://www.pymol.org/pymol

[22] Abraham, M.J., Murtola, T., Schulz, R., Páll, S., Smith, J.C., Hess, B., *et al*. (2015) GROMACS: High Performance Molecular Simulations through Multi-Level Parallelism from Laptops to Supercomputers. *Software X*, **1**, 19-25. https://doi.org/10.1016/j.softx.2015.06.001

[23] Pawar, S.S. and Rohane, S.H. (2021) Review on Discovery Studio: An Important Tool for Molecular Docking. *Asian Journal of Research in Chemistry*, **14**, 1-3. https://doi.org/10.5958/0974-4150.2021.00014.6

[24] Gu, L., Zhang, H., Song, S., Zhou, Y. and Lin, Z. (2001) Structure of an Acidic Phospholipase A2 from the Venom of *Deinagkistrodon acutus*. *Acta Crystallographica Section D Biological Crystallography*, **58**, 104-110. https://doi.org/10.1107/s0907444901018170

[25] Zheng, Q., Wang, Y. and Zhang, S. (2021) Beyond Alkaloids: Novel Bioactive Natural Products from Lobelia Species. *Frontiers in Pharmacology*, **12**, Article 638210. https://doi.org/10.3389/fphar.2021.638210

[26] Damaj, M.I., Patrick, G.S., Creasy, K.R., *et al*. (1997) Pharmacology of *lobeline*, a Nicotinic Receptor Ligand. *Journal of Pharmacology and Experimental Therapeutics*, **282**, 410-419.

[27] Decker, M.W., Majchrzak, M.J. and Arnerić, S.P. (1993) Effects of Lobeline, a Nicotinic Receptor Agonist, on Learning and Memory. *Pharmacology Biochemistry and Behavior*, **45**, 571-576. https://doi.org/10.1016/0091-3057(93)90508-q

[28] Roni, M.A. and Rahman, S. (2014) The Effects of Lobeline on Nicotine Withdrawal-Induced Depression-Like Behavior in Mice. *Psychopharmacology*, **231**, 2989-2998. https://doi.org/10.1007/s00213-014-3472-y

[29] Andreasen, J.T., Nielsen, E.Ø. and Redrobe, J.P. (2009) Chronic Oral Nicotine Increases Brain [3h] Epibatidine Binding and Responsiveness to Antidepressant Drugs, but Not Nicotine, in the Mouse Forced Swim Test. *Psychopharmacology*, **205**, 517-528. https://doi.org/10.1007/s00213-009-1560-1

[30] Bell, R.L., Eiler, B.J.A., Cook, J.B. and Rahman, S. (2009) Nicotinic Receptor Ligands Reduce Ethanol Intake by High Alcohol-Drinking HAD-2 Rats. *Alcohol*, **43**, 581-592. https://doi.org/10.1016/j.alcohol.2009.09.027

[31] Dwoskin, L.P. and Crooks, P.A. (2002) A Novel Mechanism of Action and Potential Use for Lobeline as a Treatment for Psychostimulant Abuse. *Biochemical Pharmacology*, **63**, 89-98. https://doi.org/10.1016/s0006-2952(01)00899-1

[32] Miller, D.K., Crooks, P.A. and Dwoskin, L.P. (2000) Lobeline Inhibits Nicotine-Evoked [3h] Dopamine Overflow from Rat Striatal Slices and Nicotine-Evoked $^{86}Rb^{+}$ Efflux from Thalamic Synaptosomes. *Neuropharmacology*, **39**, 2654-2662. https://doi.org/10.1016/s0028-3908(00)00140-4

[33] Miller, D.K., Harrod, S.B., Green, T.A., Wong, M., Bardo, M.T. and Dwoskin, L.P.

(2003) Lobeline Attenuates Locomotor Stimulation Induced by Repeated Nicotine Administration in Rats. *Pharmacology Biochemistry and Behavior*, **74**, 279-286. https://doi.org/10.1016/s0091-3057(02)00996-6

[34] Wei, L., Lv, S., Huang, Q., Wei, J., Zhang, S., Huang, R., *et al*. (2015) Pratensein Attenuates Aβ-Induced Cognitive Deficits in Rats: Enhancement of Synaptic Plasticity and Cholinergic Function. *Fitoterapia*, **101**, 208-217. https://doi.org/10.1016/j.fitote.2015.01.017

[35] Zhang, Q., Li, S. and Huang, Q. (2021) Pratensein Glycoside Attenuates Respiratory Syncytial Virus Infection-Induced Oxidative and Inflammatory Injury via Tgf-B Signaling Pathway. *Molecular & Cellular Toxicology*, **18**, 329-337. https://doi.org/10.1007/s13273-021-00200-2

[36] Wang, R., Wei, Y., Deng, W. and Teng, J. (2022) Pratensein Mitigates Oxidative Stress and NLRP3 Inflammasome Activation in Ogd/r-Injured HT22 Cells by Activating Nrf2-Anti-Oxidant Signaling. *Neurotoxicity Research*, **40**, 384-394. https://doi.org/10.1007/s12640-022-00472-z

[37] Liang, C., Tan, S., Huang, Q., Lin, J., Lu, Z. and Lin, X. (2015) Pratensein Ameliorates B-Amyloid-Induced Cognitive Impairment in Rats via Reducing Oxidative Damage and Restoring Synapse and BDNF Levels. *Neuroscience Letters*, **592**, 48-53. https://doi.org/10.1016/j.neulet.2015.03.003